Article type: Full Article

Title: Ultra-structural analysis of Human Spermatozoa by Aperture Scanning Near-Field Optical Microscopy

Barbara Troian[1], Rita Boscolo[2], Giuseppe Ricci[2,3], Marco Lazzarino[4], Gabriella Zito[2], Stefano Prato[1], Laura Andolfi[4*]

1 A.P.E.Research S.r.l., Basovizza, 34149 Trieste, Italy

2 Institute for Maternal and Child Health, IRCCS "Burlo Garofolo" Trieste 34137, Italy

3 Department of Medical, Surgical and Health Sciences, University of Trieste, Italy

4 Istituto Officina dei Materiali IOM-CNR, Basovizza, 34149 Trieste, Italy

*Correspondence: Laura Andolfi, IOM-CNR, Basovizza, 34149 Trieste, Italy.

E-mail:andolfi@iom.cnr.it

Abstract

Scanning near-field optical microscopy (SNOM) represents a potential candidate for investigation of ultrastructures in human spermatozoa. It is a noninvasive optical technique that offers two main advantages: minimal sample preparation and simultaneous topographical and optical images acquisition with a spatial resolution beyond the diffraction limit. This enables the combination of surface characterization and information from the inner cellular organization in a single acquisition providing an immediate and comprehensive analysis of the cellular portions. In this work spermatozoa are immobilized on poly-L-lysine coated coverslips, fixed according to a standard protocol and imaged by aperture-SNOM in air. In the SNOM images all peculiar sperm portions show well resolved optical features, which exhibit good similarities with the structures revealed in transmission electron microscopy images, as compared with literature data. The optical features of anomalous spermatozoa are clearly different as respect with those observed for healthy ones. This analysis reveals the potentialities of SNOM and opens to its application to high resolution analysis of sperm morphological alterations, which might be relevant in reproductive medicine.

Key words: scanning near-field optical microscopy, spermatozoa, infertility, reproductive medicine.

1. INTRODUCTION

The determination of the male reproductive potential is conventionally evaluated by analyzing some semen parameters, such as sperm concentration, motility, and morphology. Careful morphology evaluation and the strict application of the existing guidelines available on the World Health Organization manual (WHO 2010) [1], has a fundamental role in the clinical assessment of male fertility [2]. A common approach to evaluate the morphology of spermatozoa is light microscopy, but although very fast and rather simple has many limitations as poor resolving power and the difficulty to detect many inner alterations of sperm characteristic regions. To improve the diagnostic screening, some methods have been established based on several sperm morphology features [3-5].

The description of spermatozoa ultra-structures has been possible by using high resolution techniques as transmission electron microscopy (TEM). In general TEM has been proven to be a powerful tool in the analysis of nearly every inner cellular component, including cytoskeleton, membrane systems, organelles, flagellum and cilia. This approach, in combination with immunocytochemical assays, is important in the sperm pathology investigation to characterize the structural anomalies of defective spermatozoa [6-8]. Despite its outstanding spatial resolution, the use of TEM has two main limitations: time-consuming sample preparation and the need of staining. In this sense the ultra-structural cell analysis has benefited from the application of scanning probe microscopy (SPM), which does not require specific sample preparation or staining and it can be performed even in fluid under physiological conditions. Among the different SPMs the atomic force microscopy (AFM) is, undoubtedly, the most applied in biological investigations [9]. AFM is a versatile tool, which thanks to the ability of measuring pN forces between the probe and the sample allows to measure a wide variety of mechanical properties of living cells. Mechanical parameters measured by AFM include force, pressure, tension, adhesion, friction, elasticity, and viscosity [10, 11]. The high spatial resolution of AFM imaging (0.1 nm in z and 1 nm in x-y), comparable and even better than that of TEM, enables to visualize and evaluate the cell membrane with the possibility of revealing morphology and roughness [12]. However the inner cellular structures remain concealed for this technique.

The aperture scanning near-field optical microscopy (SNOM) provides simultaneously topographic and optical images of objects with submicrometric spatial resolution (50-200 nm). In aperture SNOM, light is shone on the sample through a subwavelength aperture, thus generating a non propagating evanescent field. In absence of a sample, no light is transmitted and the reflection signal is maximal. When the tip is approached to the sample at a distance closer than the decay length of the evanescent field, the sample interacts with the incoming light by scattering it into the far field, either in forward and backward direction (usually indicated as transmission and reflection, respectively), in general the

SNOM signal is mainly composed of scattered light. As a consequence, at first approximation, transmitted light provides similar information as dark field optical microscopy in far field, while reflected light provides similar to phase imaging, both with better spatial resolution. Apertureless SNOM, on the other hand, is based on light scattering from the tip, and its intensity depends on the tip-sample interaction. Without the need of a fiber aperture and relying on scattered rather than transmitted light, the tip size can be reduced to a few nanometers and the spatial resolution as well [13]. The price to pay is that there is not a real light-sample interaction, and since also the vertical extent of the near field is determined by the tip size, apertureless SNOM cannot be used to investigate the inner structure of a cell. Indeed apertureless SNOM finds application in the investigation of lipid membranes, cell membranes, single protein, isolated fluorophores, fibrils, DNA and other nanosized structures [14].

As for AFM, SNOM imaging on cells can be carried out in air or in liquid with very simple sample preparation. Thanks to its intrinsic capability to correlate optical signal with topographic information, it appears very promising to obtain a complete description of the cell status. The application of aperture SNOM allowed the investigation of the organization and the dynamics of fluorescent labeled protein in the plasma membrane with nanometric resolution [15,16]. By using immune-staining procedure SNOM has provided a combined description of external and cytoplasmatic structures of olygodendricytes [17]. Without the need of any specific staining SNOM has enabled the investigation of the uptake of crocidolite fiber into the cell and its interaction with subcellular organelles [18]. Likewise SNOM, in combination with an infrared free electron laser (SNOM-IR-FEL), has been used to distinguish between normal and squamous low grade and high-grade dyskaryosis, and between normal and mixed squamous/glandular pre-invasive and adenocarcinoma cervical lesions [19]. Changes in cell morphology, due to physiological reactions, could be detected in fluid SNOM imaging [20].

For the characterization of sperm morphology, AFM has been demonstrated to be relevant to obtain high resolution 3D surface topography of fixed sample [21-23]. An AFM study of mammalian spermatozoa guided in understanding cell structure–function relationship, which is expected to have a significant application in human reproduction [24]. In our previous work we have demonstrated the promising capability of SNOM to provide detailed information about the inner cellular structures of spermatozoa, without any specific labeling [25].

In this work we apply SNOM imaging on some important sperm defects associated with men infertility. SNOM images show that the sperm peculiar portions can be visualized with high spatial resolution and that the optical features reproduce the structures of spermatozoa commonly revealed

by TEM images, as compared with literature data. Remarkably the differences between the optical features of normal and anomalous spermatozoa can be clearly resolved.

2. MATERIALS AND METHODS

2.1 Sample preparation for SNOM imaging

Semen samples were obtained from two men undergoing routine infertility investigations at Assisted Reproduction Unit of the Institute for Maternal and Child Health IRCCS Burlo Garofolo, Trieste, Italy, with written informed consent. All the details about semen analysis and treatment are reported in supporting information.

One aliquot of the cells suspension was deposited on poly-L-lysine coated coverslips (24 mm diameter) (Bio Optica) and incubated at 37°C in a 5 % CO_2 atmosphere for 1h. Samples were then fixed with 4% paraformaldehyde (PFA) in PBS for 15 min at room temperature, washed three times in PBS, two times in water, partially dehydrated (up to 90% ethanol) and allowed to dry.

2.2 SNOM set-up

Aperture-SNOM imaging was performed by a TriA-SNOM microscope (A.P.E. Research, Trieste, Italy), equipped with a flexure scanning stage with a maximum xy scan range of 100 μm x 100 μm and 10 μm in z axis, with a strain gauge sensors to obtain an absolute positioning of the probe.

SNOM probe was an aluminum-coated tapered pulled optical fiber with a nominal tip aperture of 50 nm (Lovalite, Besançon, France). The fiber, mounted on a quartz sensor oscillating at its resonance frequency (30KHz), was kept close to the sample surface via shear-force feedback.

The TriA-SNOM setup is provided with interchangeable laser sources, coupled with a single mode optical fibre. In order to increase the Raleigh scattering intensity, which is proportional to $(1/\lambda)^4$, the shortest possible wavelength should be chosen. Moreover, given the aperture size, also the SNOM tip transmission increases at shorter wavelengths. However blue and near UV lights excite autoflorescence emission, creating a continuous background that blurs the image, while deeper UV is not suitable for SNOM, since there are no optical fibers transparent at those wavelengths. Therefore in this work we selected an optimal laser wavelength of 532 nm. The laser power was 20mW, but after coupling into the fiber, the radiation power transferred by the aperture of the SNOM tip was reduced to 2μW- 20nW on the sample, depending on the aperture diameter and shape of SNOM tip. For these measurements we used a narrow band-pass interference filter at 532 nm wavelength (full width-half maximum=10 ±2 nm). TriA-SNOM microscope is supplied with two integrated optical

vision systems to control the probe position and select the scan area. An upper optical vision system was used to monitor probe approach to the sample, and one transmission camera (with interchangeable achromatic objectives) was utilized for a bottom view of the sample. In these measurements an infinity corrected plan long working distance achromatic objective 20X was used. SNOM optical reflection and optical transmission signals were simultaneously detected with two photomultipliers (R74000, Hamamatsu Photonics KK Hamamatsu, Japan). The SNOM images were acquired with: 256x256 pixel and 0.1-0.4 msec acquisition time for each pixel and processed by A.P.E. Research SPM control software (A.P.E. Research, Trieste, Italy). In the high resolution images the pixel size was maintained less than 30nm, in order to sample with at least twice the spatial frequency of the tip aperture, thus satisfying the application of Nyquist theorem in scanning field microscopy [26].

2.3 Analysis of SNOM images

The analysis was carried out by Gwyddion 2.47 (http://gwyddion.net/), a free and open source software for scanning probe microscopy data visualization and analysis, covered by GNU General Public License. Gwyddion development is supported by Department of Nanometrology, Czech Metrology Institute. Some SNOM images were cropped to better highlight the spermatozoa peculiar regions. As result the image size in pixels is: 188 x 109 for Fig. 1 (C-E); 256 x 170 for Fig.2(A-C); 129 x 92 for Fig.2 (D-E) ; 156 x 203 for Fig.3(A-C); 210 x 256 for Fig.3 (D-F); 230 x 245 for Fig.4 (A-C); 256 x 114 for Fig. 5(A-C) and 256 x 163 for Fig. 5(D-F).

RESULTS AND DISCUSSION

Anomalous spermatozoa are identified by considering several morphological features. The morphological anomalies, which are related to men infertility, include head size, neck, midpiece and tail defects [2, 27]. For a spermatozoon to be classified as healthy, the whole spermatozoon has to show normal morphological features. A normal head has a regular oval shape with a length ranging between 3.0–5.0 μm and width 2.0–3.0 μm; mid-piece with a length of 5.0–7.5 μm and width of 1 μm and tail length of 45 μm. In the midpiece area is present a coiled helix of 12-13 turns of mitochondria enveloping the axoneme and the outer dense fibers, ending in the neck with a basal plate, proximal centriole and striated connecting piece detectable at the TEM level [8, 28, 29].

In this work we analysed spermatozoa with some typical sperm anomalies concerning head, neck and midpiece as identified by optical microscopy [2].

Healthy spermatozoa are identified by optical microscopy and visualized with 100X objective (Fig. 1A). At this magnification the main sperm portions can be recognized (see Fig. 1B), but their structural description is approximate due to the Abbe diffraction limit. The same sample is imaged by SNOM and representative images acquired on similar healthy spermatozoa are shown in Fig.1 (C-E). The size parameters are quantified by the analysis of the SNOM topography image (Fig. 1C): the head is evaluated to be 5μm in length and 3μm width. The front head of the spermatozoa is completely flattened due to a dehydration effect. The length of the midpiece is estimated to be 4.8μm and the width 1μm. The SNOM reflection images (Fig. 1D) recalls the surface topology observed in topography image, mainly related to the cell membrane. SNOM transmission image (Fig. 1E) provides more interesting details. Indeed it is shown that mitochondria and other organelles sized between 100nm and 1μm are responsible for scattering at large angles, whereas nuclei and cytoplamastic membrane are responsible for small-angle scattering [30]. Since, as discussed in the introduction, transmission SNOM intensity is proportional to light scattering at large angles, these images highlight the structure of subcellular and subwavelength organelles. The observed features have an organization similar to that reported in TEM images [8]: the nucleus occupies the major part of the sperm head and contains condensed chromatin; the acrosome region covers two third of the head [28,31]; the midpiece region shows a granular sequential organization which recalls the coiled helix of the mitochondria that surround the axoneme and the dense fibers, similarly to what observed in our previous work [25]. These data confirm that these optical features are reproducible and can be observed in general on the healthy spermatozoa.

A closer view of midpiece area is obtained by high resolution SNOM imaging (Fig.2A-C). In the SNOM transmission images several bright features can be observed which identify the region of centriole in the neck [28,32] and the midpiece region where mitochondria with helicoidal organization are present. In this latter region, the use of a threshold mask for the highest signal enables to better highlight a sequential grain organization and to identify 11 separated circular features (Fig. 2D), which appears to be in agreement with the number of coiled helix of mitochondria reported literature for normal spermatozoa [6]. A center-to-center separation between them is in the 300nm, range, as shown in the longitudinal profile, indicating that each one is a single mitochondrion of size less than 300nm. (Fig. 2 E,F).

SNOM imaging is then performed on anomalous spermatozoa, that fall in the group of head defects. In Fig. 3 SNOM images of a two heads spermatozoon are shown. The presence of the midpiece region cannot be detected in the SNOM topography image (3A), and even the SNOM reflection and transmission images do not display any sequential grain organization (Fig.3 B and C). At the level of head-neck, some stripes, for a few scanning lines, can be observed due to the difficulty to image this

region where folded membrane can be often found in two head-neck junction of two-head spermatozoa. Hence to better analyses the organization of the midpiece high resolution SNOM images on this region are acquired (Fig. 3D-F). The SNOM transmission confirm the absence of the grain features, suggesting that the helicoidal arrangement of mitochondria is completely lost. Both in SNOM reflection and transmission images the neck region is absent and two axoneme regions (or dense fibers) superimpose and intersect. The lateral size of the single longitudinal structures, considering the broadening due to the convolution with the aperture size, is 150-180nm as evaluated at half height in the profile of the SNOM transmission image (Fig. 3G). Moreover the depressed regions of the profile with minima positioned at approximately 1.1 and 1.9 μm, can be associated with the black contour surrounding the spermatozoa. Probably this effect is due to the topographic slope of the sample. In these regions the distance between the SNOM probe and the sample is higher as compared to other regions and the probe cannot follow the topography of the sample due to its size, which results in weaker optical signals.

Another typical head defects, is the thin head defined also as "tapered" characterized by an elongated head and thin insertion neck [2, 8, 22]. The length of the head was found of 9μm and width of 4μm, as evaluated in the SNOM topography (Fig. 4A), much longer than the common healthy one. In the SNOM topography the presence of the typical midpiece region morphology is not visible. Both in SNOM reflection and transmission images (Fig. 4B and C) we can observe numerous and evident differences with respect to the healthy one (see Fig.1): the organization at the base of the head is completely lost; the acrosome is not visible. The SNOM reflection and transmission of the midpiece region, close to the head, display a structural organization very similar to that of the spermatozoon of Fig. 3. No grain organization is visible, thus suggesting that even in this case the helicoidal organization of the mitochondria is absent, while two longitudinal structures can be distinguished. The lateral size of these structures, considering the broadening due to the convolution with the aperture size, is 170nm and 200nm as measured at half height in the profile of the SNOM transmission image of Fig. 4D. These values are close to those observed in the previous case. This indicates that in absence of the grain sequential features, which can be ascribed to mitochondria helicoidal organization, the SNOM optical imaging is able to reproducibly detect the organization of axoneme and outer dense fibers. Even in this case, as observed in Fig. 3G, we can identify depressed regions with minima positioned at approximately 0.9 and 2.0 μm, which can be associated with the black contour surrounding the spermatozoa.

The SNOM images of a spermatozoon with an anomalous neck and midpiece, defined as "thick insertion" in human sperm defects [2,8] are shown in Fig. 5. From the SNOM topography (Fig. 5A) we evaluate the size of the head, which is found in the normal range (length 5μm and width 3μm),

while the neck region is enlarged with a short midpiece (about 3μm in length and 2μm in width). The SNOM reflection image (Fig.5B) recalls the surface topography, whereas the SNOM transmission image (Fig. 5C) displays an inner organization of the midpiece region very different as compared to a normal sperm cell. The grain arrangement seems to be absent and the longitudinal structures are pulled apart. A high magnification SNOM image acquired in the neck region is shown in Fig.5 (D-F). The SNOM topography (Fig.5D) image does not display any specific structure, as well as the SNOM reflection (Fig.5E). The SNOM transmission image (Fig.5F) confirms the absence of the typical helicoidal arrangement of the mitochondria and, at the base of the head, shows a barrel structure in which each single fragment is well visible with a size that appears to be less than 100 nm, considering the broadening due to the convolution with the aperture size, as evaluated at half height in the profile shown in (Fig.5G). These features with the barrel structure located in the centriole region, resemble the segmented (striated) column immediately below the basal membrane, as detected in the longitudinal section of the neck region in the TEM images [8, 31,33].

The SNOM optical images we obtained demonstrate the capability of this technique to observe and describe the defects of atypical spermatozoa at high resolution, beyond the diffraction limit. Traditionally, the ultrastructural description of sperm morphological defects is obtained by TEM. Remarkably the optical features we observed in the SNOM images provide the same information about the typical sperm structures observed in TEM images for longitudinal section of the spermatozoa. This indicates that SNOM is able to detect and describe the structural defects in head and midpiece of the spermatozoa immobilized, fixed and dehydrated, on a glass substrate.. This straightforward sample preparation represents a notable advantage for cell imaging as compared to that required by TEM analysis. Indeed, for examination of biological samples, TEM typically includes similar dehydration and fixation protocols, followed by more complex sectioning and staining steps. Such a large number of sample manipulation may generate artifacts in the resulting images [34]. On the contrary the contrast in the SNOM optical images is generated by differences in optical properties of the cellular components, which depends only on their chemical composition and structural arrangement. Moreover SNOM imaging offers the advantage to visualize in single images all the main regions of a single spermatozoon, since the cell adhere with a longitudinal orientation on the glass coverslip. The same is not so trivial to be obtained in TEM, since the sectioning must align precisely with the cell orientation in the resin block in order to obtain a longitudinal section of the cell, which then allows to observe all the sperm regions in a single acquisition.

The analysis of sperm ultrastructures and morphology are relevant in the assisted reproductive technology protocols, since they are strictly related to the correct functioning of the sperm and for their selection in the in vitro fertilization procedure. For instance, the absence of typical neck and

midpiece organization is associated with a reduced sperm motility and as consequence with infertility [28, 35]. In this framework SNOM could be exploited to obtain a detailed description of sperm defects without the need of labeling protocol, as in optical microscopy, but with higher spatial resolution and together the topographical information. Therefore SNOM could be useful in the description of rare sperm disorder as globozoospermia, characterized by the presence of sperm with large round head, lacking acrosome [36]. It might be applied also to better characterized specific anomalous morphology at various developmental and maturation stages of germ cells as for instance the presence of vacuoles in sperm head, which have been observed by differential interference contrast [37]. Similar morphological analysis might contribute to clarify unexplained male infertility or failure of oocyte fertilization at least in some cases. The SNOM application could be extended to investigate the effects on sperm morphology of new experimental substances for male contraception, as well as to investigate the effects of chemiotherapy and radiotherapy in oncological patients.

3. CONCLUSION

We demonstrate that SNOM may offer a convenient approach to visualize and describe the structures of spermatozoa by exploiting their differences in optical properties. SNOM measurements of spermatozoa provide high resolution information regarding the organization of sperm peculiar region without any labeling treatment, thus making much easier the sample preparation for ultrastructural analysis and reducing also possible artifacts induced by labeling treatment. SNOM cannot be considered a technique that can be easily applied for diagnosis, but as TEM can be a very useful tool to characterize sperm defects in basic research.

ACKNOWLEDGMENTS

Financial supports by Health Ministry (RF-2011-02351812) Ricerca Finalizzata “Applications of Ultrastructural Cell Analysis in the Field of Reproductive Technologies” and by Regione Friuli Venezia Giulia, within the framework of “legge regionale 17/2004: Contributi per la ricerca clinica, traslazionale, di base, epidemiologica e organizzativa”, with the project “BioMec – Applicazione delle tecnologie biomeccaniche a integrazione delle metodiche tradizionali nel contesto ospedaliero” are gratefully acknowledged.

REFERENCES

[1] World Health Organization. WHO Laboratory Manual for the Examination and Processing of Human Semen. 5th edn. Geneva; 2010.

[2] V. Chang, L. Heutte, C. Petitjean, S. Härtel, and N. Hitschfeld , Comput. Biol. Med. 2017, 84, 205.

[3] R.O. Davis, D.E. Bain, R.J. Siemers, D.M. Thal, J.B. Andrew, and C.G. Gravance, Fertil Steril 1992, 58, 763.

[4] T.F. Kruger, T.C. DuToit, D.R. Franken, A.A. Acosta, S.C. Oehninger, R. Menkveld, and C.J. Lombard, Fertil. Steril. 1993, 59, 202.

[5] J.L. Yániz, S. Capistrós, S. Vicente-Fiel, C. Soler, M. Núñez de Murga, and P. Santolaria, Reprod Domest. Anim. 2013, 48, 1019.

[6] E. Moretti, G. Sutera, and G. Collodel, Syst. Biol. Reprod. Med. 2016, 62, 171.

[7] K. Chatzimeletiou, N. Galanis, A. Karagiannidis, A. Sioga, G. Pados, D. Goulis, A. Kalpatsanidis, and B. C Tarlatzis, SAGE Open Medical Case Reports 2018, 6, 1.

[8] D. Mortimer, Mol. Hum. Reprod. 2018, 24, 567.

[9] Y.F. Dufrêne, D. Martínez-Martín, I. Medalsy, D. Alsteens, and D. J. Müller, Nat. Methods 2013, 10, 847.

[10] M. Krieg, G. Fläschner, D. Alsteens, B. M. Gaub, W.H. Roos, G. J. L. Wuite, H.E. Gaub, C. Gerber, Y.F. Dufrêne, and D.J. Müller Nat. Rev. Phys. 2019, 1, 41.

[11] L. Andolfi, E. Masiero, E. Giolo, M. Martinelli, S. Luppi, S. dal Zilio, I. Delfino, R. Bortul, M. Zweyer, G. Ricci, M. Lazzarino, Integr. Biol. 2016, 8, 886.

[12] Y. Shi, M. Cai, L. Zhou, and H. Wang, Semin. Cell Dev. Biol. 2018, 73, 31.

[13] P. Bazylewski, S. Ezugwu and G. Fanchini Appl. Sci. 2017, 7, 973

[14] D. Naumenko, D. Cassese, M. Lazzarino and A. Bek F. Benfenati et al. (eds) Novel approaches for Single Molecule activation and Detection. Advances in Atom and Single Molecules Machines, Springer-Verlag Berlin Heidelberg 2014 pg. 61-83.

[15] F. De Lange, A. Cambi, R. Huijbens, B. de Bakker, W. Rensen, M. Garcia-Parajo, N. Van Hulst, and C.G. Figdor.. J Cell Sci. 2001, 114, 4153.

[16] C. Höppener, J. P. Siebrasse, R. Peters, U. Kubitscheck, and A. Naber, Biophys. J. 2005, 88, 3681.

[17] E. Trevisan, E. Fabbretti, N. Medic, B. Troian, S. Prato, F. Vita, G. Zabucchi, and M. Zweyer, Neuroimage 2010, 49, 517.

[18] L. Andolfi, E. Trevisan, M. Zweyer, S. Prato, B. Troian, F.Vita, V. Borelli, M. R. Soranzo, M. Melato, and G. Zabucchi, J Microsc. 2013, 249, 173.

[19] D.E. Halliwell, C.L.M. Morais, K.M.G. Lima, J. Trevisan, M.R.F. Siggel-King, T. Craig, J. Ingham, D.S. Martin, K.A. Heys, M. Kyrgiou, A. Mitra, E. Paraskevaidis, G. Theophilou, P.L. Martin-Hirsch, A. Cricenti, M. Luce, and P. Weightman, F.L. Martin, Sci. Rep. 2016, 6, 29494.

[20] K. Bulat, A. Rygula, E.Szafraniec, Y. Ozaki, M.Baranska, J. Biophotonics, 2017, 10, 928.

[21] S. Kumar, K. Chaudhury, P. Sen and S.K. Guha, J. Nanobiotechnol. 2005, 3, 9.

[22] P. Sunanda, B. Panda, C. Dash, R.N. Padhy, and P. Routray. Andrology 2018, 6, 680.

[23] J. O. Carvalho, L. P. Silva, R.Sartori, and M.A.N. Dode, PLOSONE, 2013, 8, e59387.

[24] S. Kumar, K. Chaudhury, P. Sen and S.K. Guha, J. Microsc. 2007, 227, 118.

[25] L. Andolfi, E. Trevisan, B. Troian, S. Prato, R. Boscolo, E. Giolo, S. Luppi, M. Martinelli, G. Ricci and M. Zweyer, J Nanobiotech. 2015, 13, 2.

[26] J. B. Heymann, C. Möller and D. J. Müller J. Microsc. 2002, 207, 43.

[27] R. Menkveld, C.A.G. Holleboom and J.P.T. Rhemrev, Asian J. Androl. 2011, 13, 59.

[28] V. Visco, S. Raffa, and J. Elia. Int. J. Urol. 2010, 17, 259.

[29] M.S. Rahman, J-S. Lee, W-S. Kwon, and M-G. Pang, Int. J. Endocrinol. 2013, 360986.

[30] J. R. Mourant, J. P. Freyer, A. H. Hielscher, A. A. Eick, D. Shen and T.M. Johnson Appl. Opt. 1998, 37, 3586.

[31] A.H. Sathananthan, S.S. Ratnam, S.C. Ng , J J. Thrin, L. Gianaroli, and A. Trounson, Hum. Reprod. 1996, 11, 345.

[32] E.L. Fishman, K. Jo, Q.P.H..Nguyen, D. Kong, R. Royfman, A.R. Cekic, S. Khanal, A.L. Miller, C. Simerly, G. Schatten, J. Loncarek, V. Mennella, and T. Avidor-Reiss, Nat. Commun. 2018, 9, 2210.

[33] E.E. Bragina and E. N. Bocharova. Ultrastructure of Spermatozoa from Infertility Patients. (2017) chapter 5. DOI: 10.5772/intechopen.71596.

[34] W-J. Zhu, Andrologia 2018, 50, e13043.

[35] P. Lhuillier, B. Rode, D. Escalier, P. Lore`s, T. Dirami, T. Bienvenu, G. Gacon, E. Dulioust, and A. Toure. Hum. Reprod. 2009, 24, 1296.

[36] G Ricci, L Andolfi, G Zabucchi, S Luppi, R Boscolo, M Martinelli, M Zweyer, and E. Trevisan. BioMed Research Int. 2015, 2015, 798754.

[37] A. Tanaka, M. Nagayoshi, I. Tanaka, and H. Kusunoki. Fertil. Steril. 2012, 98, 0015.

FIGURE LEGENDS

Figure 1: Human spermatozoa with normal features. Bright field optical image of spermatozoa with normal features as observed with a 100X objective (Zeiss) (A); sketch illustrating all the main sperm cellular structures as modified from [26] with gentle permission (B); SNOM topography (C) reflection (D) and transmission (E) images.

Figure 2: Zoomed scan area of neck and midpiece of normal sperm cell. SNOM topography (A), reflection (B) and transmission (C) images, the red circle defines the centriole region. In (D) is shown a zoomed view of SNOM transmission in (C), indicated by the yellow dotted square. The red grains identify the mask obtained by considering the highest signal intensity; the optical intensity profile (F) along the red line in (E).

Figure 3: Sperm head defects "two head". SNOM topography (A), reflection (B) and transmission (C) images. Zoomed scan area on the neck and midpiece region SNOM topography (D), reflection (E) and transmission (F) images; the white line is the optical intensity profile across the midpiece (G).

Figure 4: Sperm head defects "tapered". SNOM topography (A), reflection (B) and transmission (C) images; the white line indicates the optical intensity profile across the midpiece (D).

Figure 5: Sperm neck and midpiece defects "thick insertion". SNOM topography (A), reflection (B) and transmission (C) images. A zoomed scanned area at the level of the sperm neck: SNOM topography (D), reflection (E) SNOM transmission (F) images; the white line indicates the optical intensity profile across the segmented column (G).

Graphical Table of Contents

The Ultra-structural analysis of Human Spermatozoa by Aperture Scanning Near-Field Optical Microscopy

Barbara Troian[1], Rita Boscolo[2], Giuseppe Ricci[2,3], Marco Lazzarino[4], Gabriella Zito[2], Stefano Prato[1], Laura Andolfi[4*]

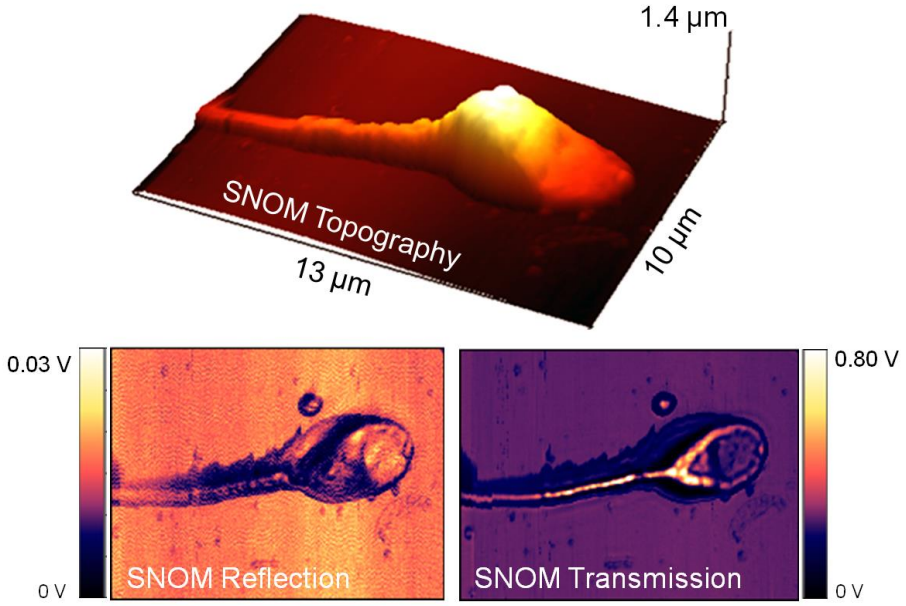

Scanning near-field optical microscopy (SNOM) represents a powerful approach for ultrastructural analyze of human spermatozoa. It is a non-invasive optical technique that requires minimal sample preparation and provides topographical and optical images simultaneously, with a spatial resolution beyond the diffraction limit. In this paper typical sperm anomalies, related to men infertility, are imaged by aperture-SNOM. The optical features of anomalous spermatozoa differ clearly from those of healthy ones and exhibit good similarities with transmission electron microscopy data from literature.